Anal. Bioanal. Electrochem., Vol. 16, No. 5, 2024, 405-422
https://www.doi.org/10.22034/abec.2024.713501

Analytical & Bioanalytical Electrochemistry

2024 by CEE
www.abechem.com

Full Paper

A Novel Sensor for Simultaneous Determination of Histamine and Uric Acid Based on Green Synthesized CuO Nanoparticles/Graphene Oxide Composite Modified Carbon Paste Electrode

Mahdieh Azizi,[1] Ali Babaei,[1,2*] and Akbar Yousefi[1]

[1]*Department of Chemistry, Faculty of Science, Arak University, Arak, Iran*
[2]*Institute of Nanoscience & Nanotechnology, Arak University, Arak, Iran*

*Corresponding Author, Tel.: +98 863 4173401; Fax: +98 863 4173406.
E-Mails: ali-babaei@araku.ac.ir ; ali.babaei08@gmail.com

Received: 21 October 2023 / Received in revised form: 11 May 2024 / Accepted: 16 May 2024 / Published online: 31 May 2024

Abstract- The present work reports a novel green synthesis of CuO nanoparticles (CuONPs) exerting an extract of the Hymenocrater Platystegius plant as a mild and non-toxic stabilizing agent. In order to obtain its applicability, a carbon paste electrode (CPE) was modified with the CuONPs and graphene oxide (GO) (CuONPs/GO/CPE) for trace determination of histamine (HIS) and uric acid (UA). The electrochemical investigations on HIS and UA were accomplished by the application of differential pulse voltammetry (DPV), cyclic voltammetry (CV), and chronoamprometry (CA) methods. The results showed the modified electrode expedites the electron transfer reactions of HIS and UA. The modified electrode exhibited some advantages such as good stability, convenient preparation, and high sensitivity toward HIS and UA determination. Under the optimum conditions, the electrode provides a linear response versus HIS and UA concentrations in the range of 1-300 and 0.5-500 µM, with a detection limit of 0.94 µM and 0.25 µM (S/N=3), respectively. The electrochemical results recommended that the CuONPs/GO/CPE is a promising sensor to determine HIS and UA in real samples with a significant recovery.

Keywords- Green synthesized copper oxide nanoparticles; Histamine; Uric acid; Graphene Oxide; Modified carbon paste electrode

1. INTRODUCTION

In the human body, histamine (HIS) is an important mediator in immediate allergic reactions and inflammation. HIS also plays an important role in gastric acid secretion, sleep regulation, and acts as a neurotransmitter. In addition, HIS is one of the components of snake venom and insect bites [1]. HIS is also found in several foods and drinks such as milk, cheese, fish, meat, wine, and vegetables [2]. High levels of HIS could have several effects on the human body like eczema, abdominal cramping, spasms of bronchi, and high blood pressure. Therefore, it is very important to detect the concentration of histamine in food, the human body, etc. Various analytical techniques have been used for HIS determination, mostly using high-performance liquid chromatography (HPLC) [3], capillary electrophoresis [4], thin-layer chromatography (TLC) [5], and surface-enhanced Raman spectroscopy (SERS) [6]. These methods frequently have some disadvantages such as long analysis time, being expensive, and tiresome sample pre-treatment steps. Nonetheless, electrochemical methods have advantages like great sensitivity, short response time, low cost, fewer interference, ease of use, and without time-consuming procedures. HIS is electrochemically capable of oxidation according to the mechanism reported previously [7]. Therefore, some electrochemical methods are developed for the determination of HIS [8,9].

Uric acid (UA) is an antioxidant that is found in animal foods such as red meat and legumes. It is one of the end products of purine metabolism and is existent in biological such as urine and blood. UA level abnormalities indicate the possibility of various diseases including gout, kidney disease, Alzheimer's and Multiple sclerosis (MS), Parkinson's disease, hypertension, and cardiovascular disease [10]. Therefore, monitoring the concentration of UA in human body fluids as a precaution against the above diseases or similar cases is clinically significant. Despite many efforts to identify UA such as enzymatic assay [11], HPLC [12], Mass spectrometry [13], electrophoresis (CE) [14], quantitative luminescence [15], and colorimetry [16,17] have been reported. UA is an electrochemical active compound; therefore, some electrochemical methods have been reported on UA electrochemical determination [18,19].

Often for treated diseases that are caused by excess uric acid in the body, such as gout, prescribed drugs that prevent inflammation inhibit the release of histamine from mast cells, causing pain-relieving effects. Therefore, it is important to have an electrochemical sensor that can detect and measure uric acid and histamine simultaneously.

Chemical methods are often used to prepare nanoparticles. The disadvantages of chemical reduction methods are the toxicity of chemical-reducing agent and their high cost [20-24]. Therefore, the production of nanoparticles using the principles of green chemistry by using plants and agricultural products as renewable and inexpensive sources has found a special place in research. The extract of the Hymenocrater Platystegius plant has many compounds that contain biologically active polyphenols, proteins, terpenoids, alkaloids, sugars, phenolic acids,

flavonoids, and anthocyaproducingnins which lead to its high reducing ability. The presence of hydroxyl groups of phenolic compounds in the extract of this plant has two important roles, the first role is to reduce the ability of various metal ions and the second role is as a stabilizer of nanoparticles [25,26]. It should be noted that the synthesized nanoparticles could be re-oxidized due to their high activity. Therefore, in this work, the extract of the Hymenocrater Platystegius plant was used for the first time to form CuO nanoparticles.

Carbon nanostructures have been greatly investigated due to their excellent chemical and physical possessions along with numerous applications [27,28]. Graphene oxide (GO) consists of graphene sheets with hydroxyl, epoxide, and carboxyl groups but the precise construction of GO is hard to determine [29,30]. GO usually was synthesized by exfoliation of graphite with strong oxidizing agents.

This is the first report on the fabrication of CuO nanoparticles (CuONPs) using an extract of the Hymenocrater Platystegius plant as a stabilizer of nanoparticles. In addition, there is no report on the simultaneous determination of HIS and UA. In the present work, we report an application of the green synthesized CuONPs in the fabrication of a modified carbon paste electrode with GO (CuONPs/GO/CPE) to obtain an appropriate sensor for simultaneous detection of HIS along with UA. This modified electrode displayed a lower detection limit and great sensitivity with a suitable linear range. This modified electrode was applied to detect the HIS and UA in real samples also satisfactory results were obtained.

2. EXPERIMENTAL SECTION

2.1. Chemicals and reagents

HIS and UA were purchased from Merck and Sigma chemical companies, respectively. Copper sulfate ($CuSO_4.\ 5H_2O$) was obtained from Merck. Most of the chemicals were analytically graded and they were used as received. Stock standard solutions of 10 mM UA and 10 mM HIS were made in 0.1 M phosphate buffers with a pH of 7. Phosphate buffer solutions (PBS) are making preparations with a suitable amount of stock solutions of 0.1 M NaH_2PO_4 and 0.1 M Na_2HPO_4. The most of electrochemical tests on UA and HIS were achieved in 0.1 M PBS at pH of 7, otherwise stated.

The Hymenocrater Platystegius flowers were obtained from the Arak suburb in Iran. The plant flowers and leaves were initially rinsed with deionized water thereupon it was dried in the shade at room temperature. About 10 gr of plants were ground (by Electric mill) initially, then stirred with 150 mL deionized water at 90 ºC for 60 min and filtered to obtain the extract.

2.2. Synthesis of graphene oxide (GO)

Graphene oxide (GO) was produced by using a modified Hummer's method [31]. Briefly, a 360:40 mL (9:1) combination of concentrated H_2SO_4 and H_3PO_4 was added to 3.0 g graphite

and stirred slowly. Subsequently, 18.0 g $KMnO_4$ was added gently then the solution was heated up to 50 °C while stirred for 12 h. Afterward, the solution was cooled to room temperature. Then 3 ml cold H_2O_2 with 400 ml frozen deionized water was added to it and stirred vigorously to obtain the yellow color solution. Then the deposit was centrifuged, and the remained solid material was washed in succession with deionized water, HCl (2M), and ethanol three times, respectively. Finally, the precipitate was followed by filtration and then vacuum-dried at 70 °C for 12 h to obtain a brown powder of graphene oxide.

2.3. Synthesis of CuO nanoparticles

CuO nanoparticles (CuONPs) were prepared by the green method. A solution of 50 ml (1:1) of the Hymenocrater Platystegius plant extract as reducer and stabilizer was added to the solution of 0.1 M aqueous $CuSO_4$. Then the solution was stirred rapidly thereupon heated to 80 °C for 15 min to obtain CuO nanoparticles colloids. After that, the solution was centrifuged at 1800 RPM for 20 min. The obtained precipitate was rinsed two times with ethanol also deionized water and then filtered, the deposit was initially vacuum-dried at 80 °C for 2h and then calcined in the oven at 700 °C for five hours to obtain CuONPs.

2.4. Equipments

All the voltammetric measurements were achieved by CuONPs/GO/CPE as the working electrode, Ag/AgCl 3 M KCl as the reference electrode, and platinum wire as a counter electrode. Cyclic voltammetry (CV), differential pulse voltammetry (DPV) chronoamperometry (CA), and the electrochemical impedance spectroscopy (EIS) experiments were carried out by Autolab PGSTAT 30 Potentiostat/Galvanostat (EcoChemie, The Netherlands). The pH determinations were carried out using a Metrohm 744 pH meter with a combination glass electrode. The morphological analyses were performed by Sigma VP Zeiss-scanning electron microscope (SEM). Fourier transform infrared (FT-IR) spectra were recorded as pressed KBr discs using a Unicom Galaxy Series FT-IR 5000 spectrophotometer. The XRD patterns were obtained by X-ray diffraction instrument (PHILIPS, model PW3040/60). The UV-visible spectrophotometer double-beam was from Analytic Jena company (model SPECORD 250).

2.5. Fabrication of CuONPs/GO/CPE

The modified carbon paste electrode was fabricated by grinding appropriate amounts of GO and CuONPs and graphite powder with two drops of nujol oil in the mortar until a homogenous paste was attained. Then this paste was packed firmly into a narrow syringe with an internal radius of 3 mm. Then a copper wire in the middle of the packed syringe was inserted

to act as an electrical conductor. Before use, the CuONPs/GO/CPE was polished on a portion of weighing paper and washed with distilled water to obtain a smooth surface.

2.6. General methods of analysis

The common procedure applied to get voltammograms was as follows. Each one of our sample solutions (10 mL) containing 0.1 M PBS at a pH=7.0 and a suitable quantity of analytes was added into a voltammetric cell before running any experiment. The voltammograms displayed oxidation peak potentials of approximately 0.2 V and 1 V related to UA and HIS, respectively. Prior to starting any electrochemical investigation, the solution was stirred for 80 seconds.

EIS experiments were achieved in a solution including 4 mM of each of $Fe(CN)_6^{3-}$ and $Fe(CN)_6^{4-}$ and 0.1 M KCl with the frequency range between 10^5 to 0.01 Hz.

3. RESULTS AND DISCUSSION

3.1. Characterization of CuONPs

FESEM was used to obtain a structural characterization of CuONPs (Figure 1). Figure 1a and Figure 1b show CuONPs have an average thickness of 62.79 nm. The low dimensions of the particles provide a high surface area for synthesized CuONPs. Therefore, the combination of CuONPs and porous GO suggests high anodic peak currents of the analytes with high efficiency for the modified CPE.

The elements constituent of CuONPs were revealed by EDS measurement as shown in Figure 1c. As can be seen, the EDS result confirms that only elements of Cu and O are present in the sample.

The XRD Pattern of CuONPs is demonstrated in Figure 1d. The X-ray diffraction pattern was obtained with Cu Kα radiation as the X-ray source, which was recorded in the range of 2θ = 10-85°. The results show that a few of the corresponding peaks at 29.559, 36.426, 42.304, 61.393, 73.53, and 77.34 are by JCPDS No. 01-078-2076 which belong to Cu_2O nanoparticle. In addition, the relevant peaks at 35.506, 38.714, 61.39,66.14, and 67.98 are consistent with JCPDS No. 00-041-0254 which belong to CuO that all of them are tagged in Figure 1d. Therefore, it seems that during the synthesis the mixture of two oxidation states of copper oxide would be obtained which is by previous reports [32,33].

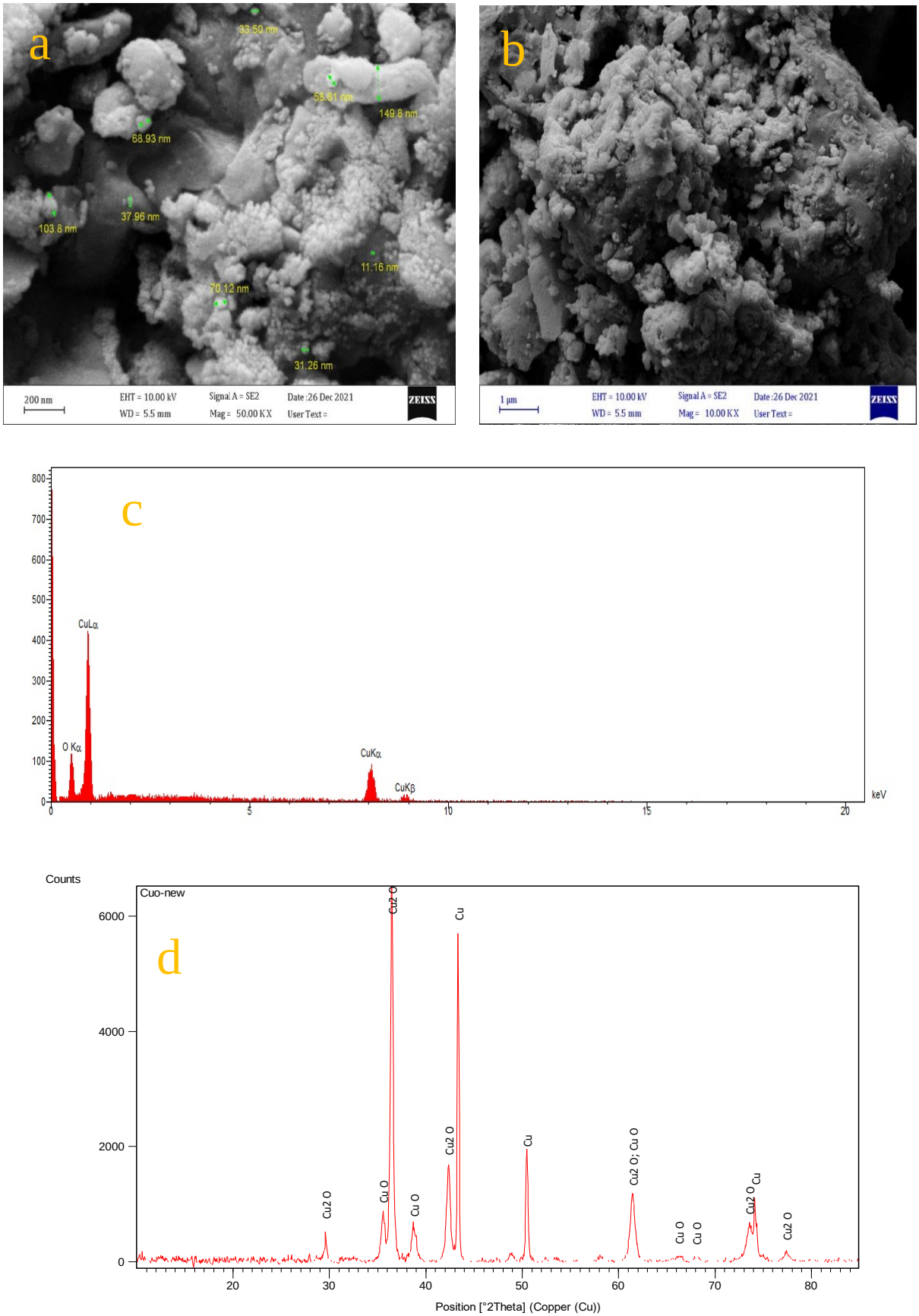

Figure 1. FESEM images of CuONPs with different resolutions (a), (b); EDS analysis of the CuONPs (c) and XRD analysis of the CuONPs (d)

FT-IR spectrum of the Hymenocrater Platystegius extract (Figure 2a) demonstrates the functional groups of its polyphenolics that are perhaps responsible for the reduction of metal ions and the formation of nanoparticles [34].

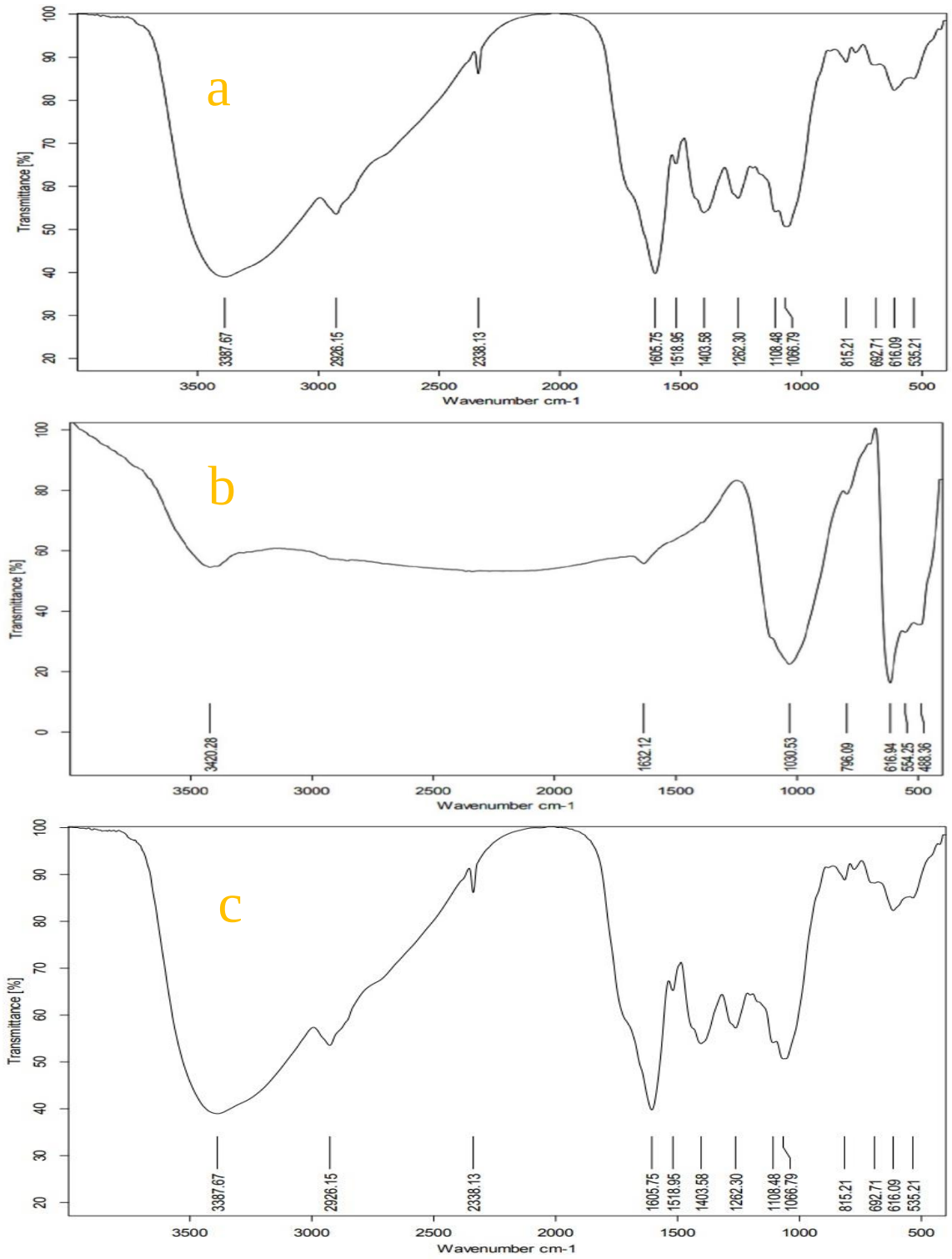

Figure 2. The FTIR spectra of Hymenocrater Platystegius extract (a), CuONPs (b), and GO (c)

A wide peak at 3387.67 cm^{-1} exhibited the (O—H) functional groups in flavonoids and folic acid. The band at 2926.15 cm^{-1} is related to the vibration =C-H and –C-H in the desired compound. In addition, signals illustrated at 2338.13, and 1605.75 cm^{-1} are relevant to saturated hydrocarbon and carbonyl groups (C=O) respectively. The absorption band 403.58 cm^{-1} is related to the tensile vibration of C-C and the absorption band 1066.79 cm^{-1} is also related to the tensile vibration of C-O [22]. The FT-IR spectrum of CuONPs is indicated in (Figure 2b) which the presence of the peak in 3420 cm^{-1} relating to tensile bonding of the hydroxyl functional group. Absorption peak around 1632 cm^{-1} is generally related to the carbonyl residues of the amino acid in the extracted protein. The absorption band observed at 554 and 616 cm^{-1} is related to the tensile vibration of the bond (Cu—O), which confirms the formation of copper oxide nanoparticles from green synthesis with the Hymenocrater Platystegius flowers extract [35,36]. Figure 2c displays the FT-IR spectrum of GO with the wide absorption band at 3389 cm^{-1} corresponding to (O—H) functional groups. The presence of the peak in 1741 cm^{-1} relates to C=O stretching vibration, peak in the range of 1624 relates to tensile vibrations (C=C) of the double bond of a hexagonal ring. These three bands approve the main and hexagonal structure of graphene oxide. However, the peaks in the range of 1227 to 1044 cm^{-1} correspond to the (C—O) epoxy group and (C—O) bond in the alkoxy group in GO. Peaks in the areas 1419 and 1374 cm^{-1} show the vibrations caused by CH_3 and CH_2, respectively. A similar spectrum was observed previously [29,32].

The UV-Vis spectra of the Hymenocrater Platystegius flower extract (Figure 3a) show absorption bands at about 273 and 330 nm that are related to the transfer $\pi \rightarrow \pi^*$. These absorption bands indicate the presence of polyphenol acids that act as antioxidants and stabilizers in the synthesis of green nanoparticles [22,37]. The results of the UV spectrum (Figure 3b) reveal an absorption band of about 300 nm that confirmed the forms of copper oxide nanoparticles [38].

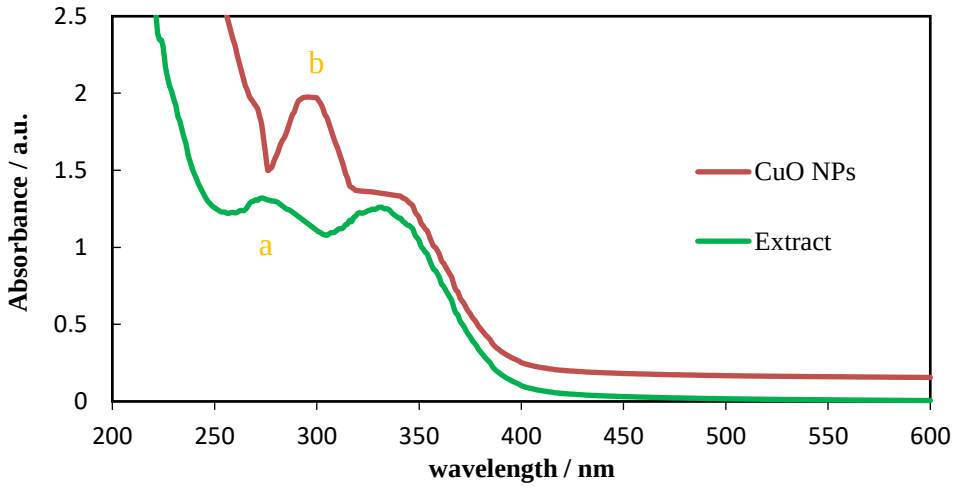

Figure 3. The UV-Vis spectra of Hymenocrater Platystegius aqueous extract (a), CuONPs (b)

3.2. Electrochemical impedance spectroscopy (EIS)

EIS can offer some information about impedance variation of the electrode surface due to the modification procedure. Figure. 4 displays the Nyquist plots (-z″ vs. z′) for CPE (Figure 4a) and CuONPs/GO/CPE (Figure 4b) electrodes achieved once the electrodes were put in a 0.1 M KCl solution including 4 mM in both $K_3[Fe(CN)_6]$ and $K_4[Fe(CN)_6]$. The diameter of the arc for the CuONPs/GO/CPE is narrower than that of the CPE, which proposes the CuONPs/GO/CPE electrode offers smaller electron transfer resistance.

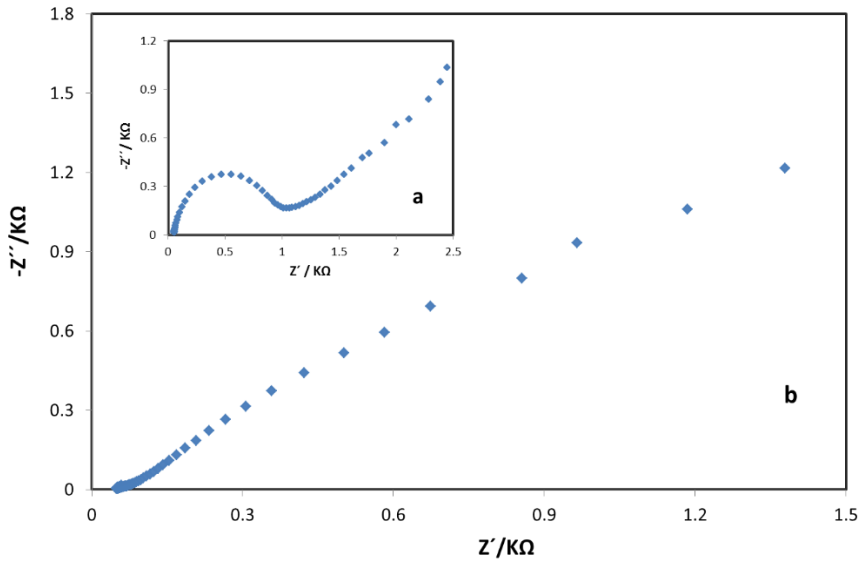

Figure 4. Nyquist plots for CPE (a), CPE modified with 8% CuONPs and 8% GO (b) electrodes obtained when the electrodes were immersed into solutions of 4 mM $K_3[Fe(CN)_6]/K_4[Fe(CN)_6]$ and 0.1M KCl solution.

3.3. Electrochemical investigations of UA and HIS on GO/ CuONPs/ CPE

The DPV results revealed that the oxidation peak currents of UA and HIS are dependent on the percentage of CuONPs and GO in the modified electrode. To optimize the percentage of the components several DPV experiments were carried out. The best results were obtained at the percentage of 8% for both GO and CuONPs in the modified electrode (Supplementary material, Figure S1, and Figure S2).

Figure 5. shows the results of DPV results at bare and modified CPE in 20 ml PBS (pH = 7). The results were obtained in a solution of 200 µM UA and 200 µM HIS at (a) bare CPE, (b) GO /CPE, and (c) CuONPs/ GO /CPE. According to the data, the highest oxidation peak currents were obtained at CuONPs/GO/CPE, leading to excellent sensitivity of the modified electrode in the simultaneous determination of HIS and UA.

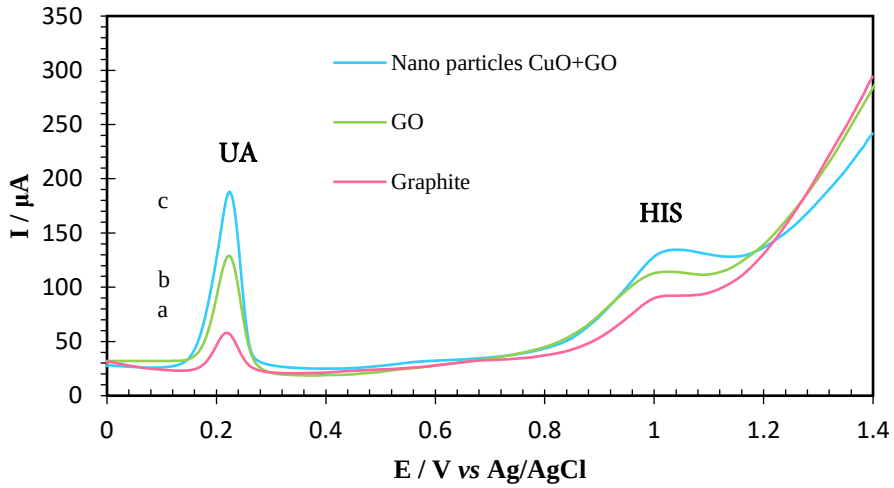

Figure 5. Differential pulse voltammograms (DPVs) with a scan rate of 0.015 v/s for concentrations of 200 µL of uric acid and 200 µL of histamine in phosphate buffer 0.1 M with pH=7.0 on unmodified CPE (a), CPE modified with GO (b) and CPE modified with GO and CuONPs (c)

The outcome of modification of the electrode active surface area was examined by CV method using 4 mM $K_3Fe(CN)_6$ in PBS (pH=7) (Supplementary material, Figure S3). Cyclic voltammograms of $K_3Fe(CN)_6$ showed a couple of reversible redox peaks at bare and modified CPEs. These results indicate that the redox peak currents at the modified electrode are higher than the bare CPE. The results showed, under similar conditions, the corresponding cathodic peak current is linear concerning the square root of the scan rate ($\upsilon^{1/2}$) at both bare and modified CPE in the scan rate range of 10-100 mVs^{-1} (Supplementary material, Figure S4). The results indicate that the electron transfer at both electrodes is under diffusion control and follows the Randles–Sevcik relationship:

$$I_p = (2/69 \times 10^5)\, n^{3/2}\, A\, C_o\, D^{1/2}\, \upsilon^{1/2}$$

According to the Randles–Sevcik equation and comparing the slope of the corresponding regression equations, the ratio of the surface area of modified electrodes of CuONPs/ GO /CPE and GO/CPE were about 7.1 and 4.8 times higher than the unmodified CPE, respectively. As a result, the highest electrochemical surface area was obtained at CuONPs/ GO /CPE due to the presence of CuONPs/ GO composite at CPE which leads to higher electrochemical response at the modified electrode.

3.4. Optimization of operating parameters

3.4.1. Effects of Electrolytes and pH

To examine the effect of the type of electrolytes on electrochemical oxidations of HIS and UA, several buffers such as phosphate, citrate, acetate, ammonia, and Briton-Robinson solution

with a concentration of 0.1 M at pH of 7 were prepared. The results of DPV experiments revealed that HIS and UA produce higher oxidation peak currents in PBS (not shown). Therefore, PBS was chosen as the best electrolyte for investigation.

The effect of pH on the response of the proposed sensor was studied by measuring the oxidation peak currents of 200 µM UA and 200 µM HIS in 0.1 M PBS in the pH range of 3 to 8 (Figure 6). The results of the experiments (Figure 6a) showed that the oxidation peak current of UA and HIS improves with increasing pH in the range of 3 to 7 and reaches to its maximum value at pH = 7, but at higher pH, the corresponding oxidation peak currents decrease. As a result, PBS with a pH of 7 was elected as the optimum pH for additional experiments. Figure 7b indicates a correlation between oxidation peak potentials of UA and HIS with pH. The results showed that by the change of pH, the resultant oxidation peak potentials for UA and HIS change directly with pH as follows:

E_{pa} = 1.556 - 0.0641 pH (R^2 = 0.9845) **HIS**

E_{pa} = 0.629 - 0.0616 pH (R^2 = 0.9614) **UA**

The equations showed the slopes near the Nernstian value which recommends the same number of proton and electron transfers are engaged in the electrochemical oxidations of UA and HIS [40,41].

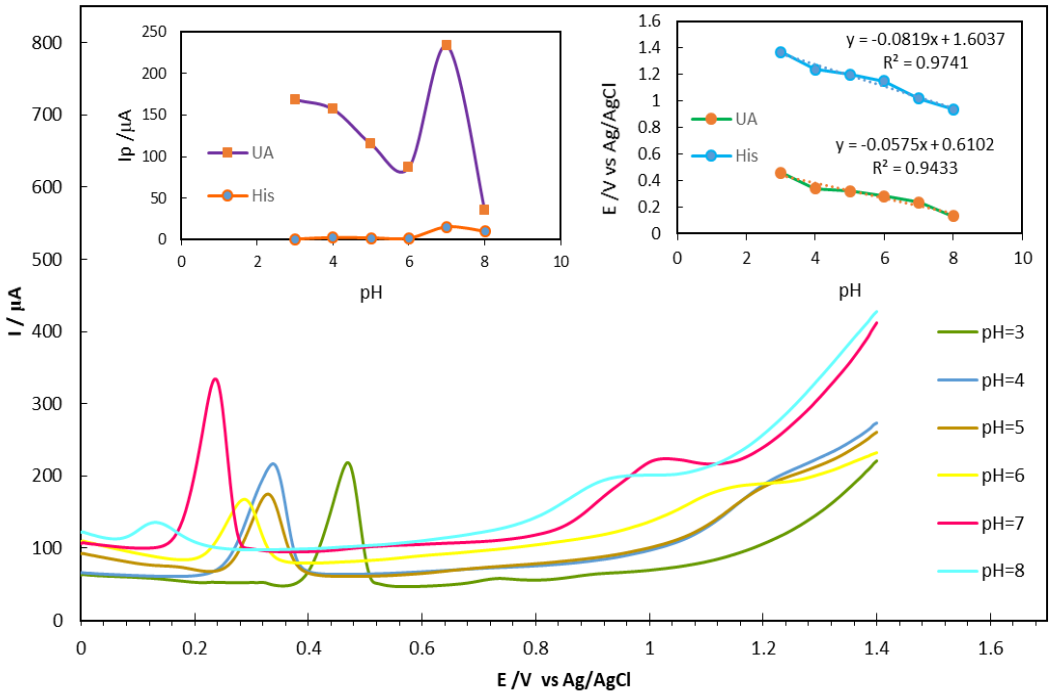

Figure 6. Differential pulse voltammograms (DPV) of 200 µM UA and 200 µM HIS compounds at CuONPs /GO/CPE in 20ml, 0.1 M phosphate buffer solution at different pH: 3, 4, 5, 6, 7, 8. Insets: (a) Plot of UA and HIS anodic peak currents (Ipa) as a function of pH values. (b) Plot of potential values as a function of pH values

3.4.2. Effects of Accumulation Time

One of the factors that affects on response of the modified electrode toward oxidation of UA and HIS is accumulation time due to its effect on the adsorption of the analytes. To obtain the best accumulation time, DPV experiments were carried out in the solution of 200 µM UA and 200 µM HIS with 0.1 M PBS (pH = 7) at the modified electrode in the accumulation time range of 0 to 120 s. As the results show (Supplementary material, Figure S5), the oxidation peaks current of UA and HIS grows with increasing accumulation time up to 80 seconds. At a longer time, saturation of the electrode surface occurs by the adsorbed compounds, and the corresponding anodic peak currents remain almost constant. According to the results, the time of 80 seconds was chosen as the most appropriate accumulation time for subsequent experiments.

3.5. Linear dynamic range and detection limit of the method

To evaluate the linear relationship between, oxidation peak currents of UA and HIS concentrations, DPV techniques were used at CuONPs/GO/CPE under optimum conditions, and the corresponding calibration diagrams were obtained (Figure 7).

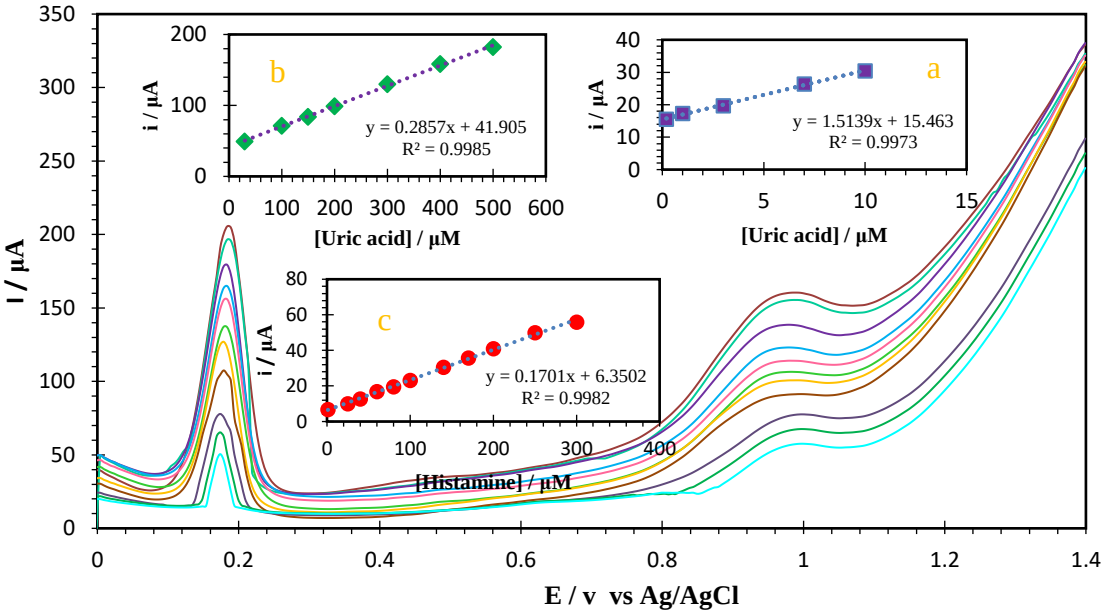

Figure 7. Differential pulse voltammograms for different concentrations of UA and HIS mixture as (a) 0.5 + 1, (b) 5 + 10, (c) 10 + 20, (d) 20 + 40, (e) 40 + 70, (f)120 + 100 (g) 150+120 (h) 200+140 (i) 300+200 (j) 400+250 and (k) 500+300 respectively, in which the first value is the concentration of UA in µM and the second value is the concentration of HIS in µM. Insets: (a) Plot of peak currents as a function of UA concentration from 0.5 until 10 µM, (b) Plot of peak currents as a function of UA concentration from 30 until 500 µM, (c) Plot of the peak currents as a function of HIS concentration.

For UA a first linear dynamic range from 0.5 µM to 10 µM with a calibration equation of Ip (µA) = 1.5139 C (µM) + 15.463 (R^2 = 0.9973), and the second linear dynamic range was between 30 to 500 µM with a calibration equation of Ip (µA) = 0.2857 C (µM) + 41.905 (R^2=0.9985) that a detection limit of 0.25 µM was obtained. For HIS a linear dynamic range from 1 µM to 300 µM with a calibration equation of Ip (µA) = 0.1701C (µM) + 6.3502 (R^2= 0.9982), and a detection limit of 0.64 µM was obtained. The literature survey showed that this is the first report on the simultaneous determination of HIS and UA using a novel sensor based on green synthesized CuONPs, which offer a wide linear dynamic range and low limit of detection.

3.6. Stability and Repeatability of the Electrode

With the intention of estimating the stability of the modified electrode in solution, the decrease in peak currents was measured by determining during repetitive DPV determinations of UA and HIS after the modified electrode was placed in 0.1 M PBS with a pH of 7 for a specific period of time. The oxidation peak currents of UA and HIS on the modified electrode after eight times measurements during 9 hours showed only a 2.6% and 5.1% decrease in corresponding oxidation peak currents, respectively. These results indicate good stability of the modified carbon paste electrode under wet conditions. To obtain stability of the modified electrode under dry conditions, the modified CPE was stored in the air for a specific period of time. After 7 days, the anodic peak current of 200 µM UA and 200 µM HIS were measured using the DPV method in 0.1 M PBS at a pH of 7. The results indicated that the oxidation peak currents of UA and HIS decreased only about 3.4% and 8.5%, respectively. The results indicate the appropriate stability of the CuONPs/GO/CPE as a new sensor for simultaneous measurement of UA and HIS in long-term applications.

To assess the repeatability of the method, repetitive DPV measurements were performed in a solution of 200 µM UA and 200 µM HIS in 0.1 M PBS with a pH of 7. The results of eight consecutive determinations indicated good reproducibility with a relative standard deviation (RSD) of 2.2 % for UA and 2.6 % for HIS, respectively. A small RSD value corroborates that the modified electrode is repeatable after successive measurements and, of course, has good accuracy too, and is not affected by contamination of UA and HIS oxidation products during voltammetric determinations. According to the results, the CuONPs/GO/CPE was not subjected to surface fouling during the voltammetric analysis which led to the sensor showing outstanding repeatability.

3.7. Chronoamperometric measurements

The diffusion coefficient (D) of UA and HIS at CuONPs/GO/CPE can also be measured by the chronoamperometry technique (Figures 8a and 8b). Chronoamperometric measurements were achieved at the modified electrode by applying separate potentials of 300 mV and 1200

mV for UA and HIS, respectively. According to the Cottrell equation [42], currents due to electrochemical reactions for an electroactive compound with a diffusion coefficient of D, are defined as follows:

$$I = n\,FA\,C\,D^{½}\,t^{-½}\,\pi^{-½}$$

In this equation, C_b and D are the bulk concentration (mol cm^{-3}) and diffusion coefficient (cm^2 s^{-1}), respectively. In situations where there is a diffusion control (mass transport), a plot of I vs. $t^{-1/2}$ is linear, and the amount of D can be attained from its slope.

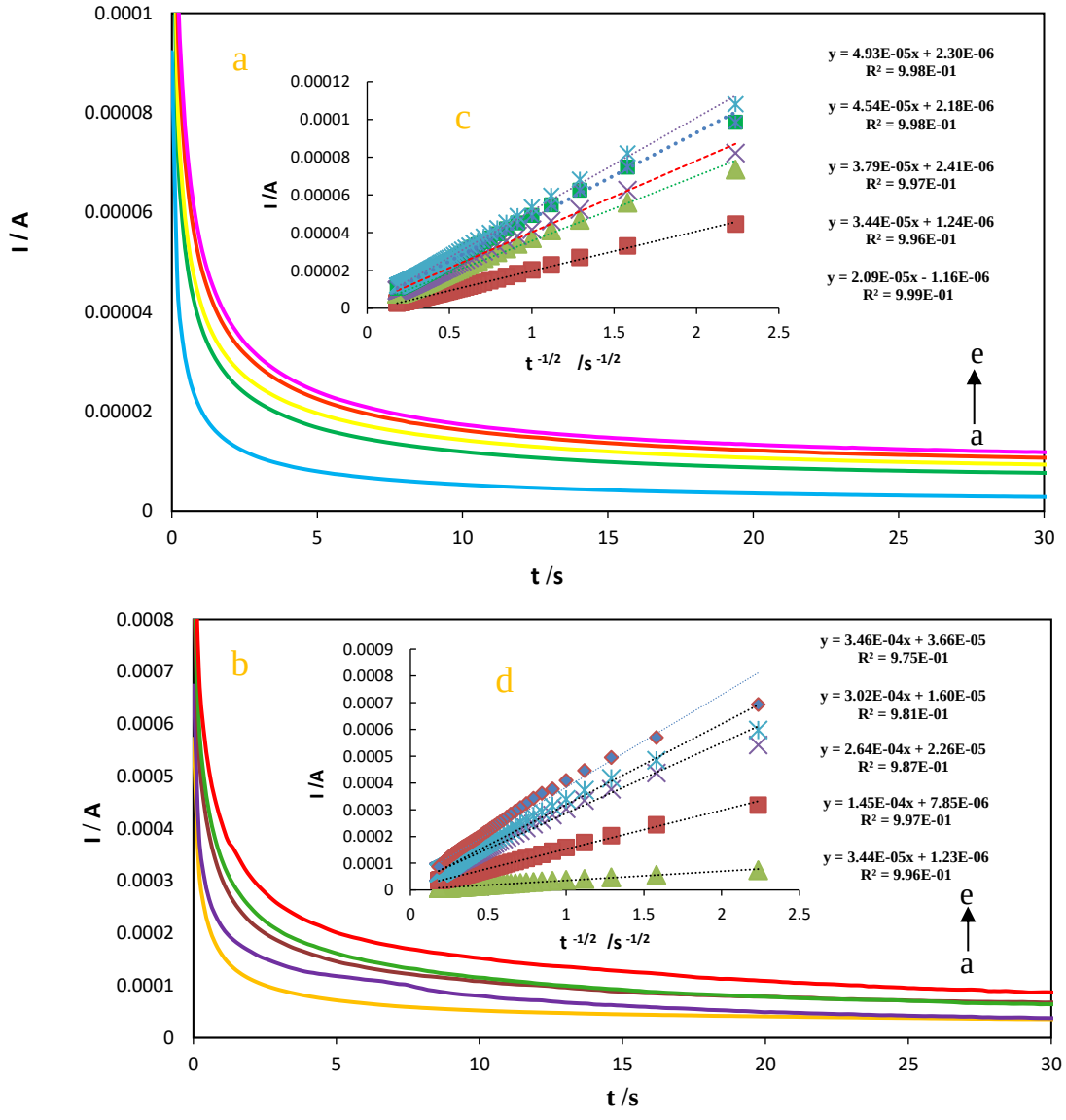

Figure 8. (a) Chronoamperograms obtained in 0.1 M phosphate buffer solution (pH= 7.0) in the (a) 100, (b) 200, (c) 300, (d) 400, and (e) 500 µM of UA at CuONPs/GO/CPE; (b) Chronoamperograms were obtained in 0.1 M phosphate buffer solution (pH=7.0) in the presence of (a) 100, (b) 200, (c) 300, (d) 400, and (e) 500 µM of HIS at CuONPs/GO/CPE. Insets: (c) Plots of I vs. $t^{-1/2}$ obtained from chronoamperograms in (a) for UA and (d) Plots of I vs. $t^{-1/2}$ obtained from chronoamperograms in (b) for HIS

Figures 8c and 8d show I-t $^{-1/2}$ diagrams of five different concentrations of UA and HIS, respectively. By using the Cottrell equation and the slopes related to these diagrams, the diffusion coefficients for UA and HIS were calculated as 1.05×10^{-5} cm^2 s^{-1} and 1.93×10^{-5} cm^2 s^{-1}, respectively.

3.8. Effect of Interferences

In Table 1, the results of the effects of some possible interferences of different species on the oxidation peak currents of 200 μM UA and 200 μM HIS on the GO/CuONPs/CPE in a solution of 0.1 M PBS with pH of 7 are given under the optimum conditions. The concentrations presented in this Table represent the concentrations of the interference (C_{Int}), which gives an error of ≤ 5% in measurements of UA and HIS. The data showed that interferences are only noteworthy at relatively high concentrations which confirms that the suggested method is expected to be free from interferences from common components with high selectivity.

Table 1. Maximum tolerable concentration of interfering species

Interfering species	UA C_{int}/ (μM)	HIS C_{int}/ (μM)
Glucose	800	550
Tyrosine	400	350
Tryptophan	550	300
Cysteine	450	350
Acetaminophen	300	350
Ascorbic acid	350	450
Na^+	650	450
Mg^{2+}	400	450
SO_4^{2-}	450	550

3.9. Analytical Applications

The analytical application of the proposed sensor was examined by measurement of UA and HIS in human serum and urine samples. The results of DPV experiments in the measurements of UA and HIS in human urine and serum are summarized in Table 2 and Table 3, respectively. Before analysis, the serum and urine samples were diluted 40 times and spiked with suitable amounts of UA and HIS. To calculate the concentrations of UA and HIS, the method of standard additions was used. The results indicate that the suggested technique is a trustworthy technique for the direct simultaneous determination of UA and HIS in real samples like biological fluids.

Table 2. Estimation of UA and HIS in diluted (40-fold) urine

Spiked (µM)		Found (µM)		[a]R.S.D. (%)		Recovery	
UA	HIS	UA	HIS	UA	HIS	UA	HIS
0	0	44.21	0	2.6	0	-	-
30	30	73.32	28.73	2.6	3.8	97.03	95.76
60	60	107.23	59.36	1.9	2.4	105.03	98.93

[a] Average of five determinations at optimum conditions

Table 3. Estimation of UA and HIS in diluted (40-fold) serum

Spiked (µM)		Found (µM)		[a]R.S.D. (%)		Recovery	
UA	HIS	UA	HIS	UA	HIS	UA	HIS
0	0	36.7	0	3.4	0	-	-
40	40	77.53	38.47	3.5	4.2	102.07	96.17
80	80	120.48	83.02	2.4	3.7	104.72	103.77

[a] Average of five determinations at optimum conditions

4. CONCLUSION

In this study, for the first time, the green synthesis of CuONPs with the Hymenocrater Platystegius plant extract is reported. To explore the application of CuONPs, it was used with GO to fabricate CuONPs/GO/CPE as a novel sensor for simultaneous measurement of UA and HIS. The results of interfering investigations of some species displayed no major interference with the determination of UA and HIS. Application of the suggested sensor for the determination of UA and HIS in some real samples gave suitable results, without the requirement of sample pretreatments or laborious extractions. The reproducibility, high stability, high speed, simplicity, low detection limit, and wide linear dynamic range, propose that the suggested sensor is an attractive candidate for real sample analysis.

Acknowledgments

The authors gratefully acknowledge the research council of Arak University for providing financial support for this work.

REFERENCES

[1] A.M. Mahdy, and N.R. Webster, Anaesth. Intensive Care Med. 12 (2011) 324.
[2] L.Y. Zhang, and M.X. Sun, J. Chromatogr. A 1040 (2004) 133.
[3] J.L. Ordóñez, A.M. Troncoso, M.D.C. García-Parrilla, and R.M. Callejón, Anal. Chim. Acta 939 (2016) 10.
[4] L. He, Z. Xu, T. Hirokawa, and L. Shen, J. Chromatogr. A 1482 (2017) 109.
[5] Z. Bajc, and K. Gačnik, JPC-Journal Planar Chromatogr. TLC 22 (2009) 15.
[6] T. Janči, D. Valinger, J.G. Kljusurić, L. Mikac, S. Vidaček, and M. Ivanda, Food Chem. 224 (2017) 48.
[7] H. Degefu, M. Amare, M. Tessema, and S. Admassie, Electrochim. Acta 121 (2014) 307.
[8] A. Veseli, M. Vasjari, T. Arbneshi, A. Hajrizi, Ľ. Švorc, A. Samphao, and K. Kalcher, Sens. Actuators B Chem. 228 (2016) 774.
[9] N. Kumar, and R.N. Goyal, Sens. Actuators B Chem. 268 (2018) 383.
[10] M.K. Kutzing, and B.L. Firestein, J. Pharmacol. Exp. Ther. 324 (2008) 1.
[11] Y. Zhang, G. Wen, Y. Zhou, S. Shuang, C. Dong, and M.M.F. Choi, Biosens. Bioelectron. 22 (2007) 1791.
[12] S.K. George, M.T. Dipu, U.R. Mehra, P. Singh, A.K. Verma, and J.S. Ramgaokar, J. Chromatogr. B 832 (2006) 134.
[13] X. Dai, X. Fang, C. Zhang, R. Xu, and B. Xu, J. Chromatogr. B 857 (2007) 287.
[14] H.L. Lee, and S.C. Chen, Talanta 64 (2004) 750.
[15] J. Yu, L. Ge, J. Huang, S. Wang, and S. Ge, Lab Chip 11 (2011) 1286.
[16] N. Kageyama, Clin. Chim. Acta 31 (1971) 421.
[17] X. Chen, J. Chen, F. Wang, X. Xiang, M. Luo, X. Ji, and Z. He, Biosens. Bioelectron. 35 (2012) 363.
[18] A. Babaei, M. Aminikhah, and A.R. Taheri, Sens. Lett. 11 (2013) 413.
[19] T. Fukuda, H. Muguruma, H. Iwasa, T. Tanaka, A. Hiratsuka, T. Shimizu, K. Tsuji, and T. Kishimoto, Anal. Biochem. 590 (2020) 113533.
[20] B. Khodadadi, J. Sol-Gel Sci. Technol. 80 (2016) 793.
[21] M. Bordbar, Z. Sharifi-Zarchi, and B. Khodadadi, J. Sol-Gel Sci. Technol. 81 (2017) 724.
[22] M. Asadipour, and M. Taherkhani, Pharm. Chem. J. 56 (2023) 1650.
[23] M. Bordbar, N. Negahdar, and M. Nasrollahzadeh, Sep. Purif. Technol. 191 (2018) 295.
[24] M. Bordbar, S. Jafari, A. Yeganeh-Faal, and B. Khodadadi, J. Iran. Chem. Soc. 14 (2017) 897.
[25] B. Khodadadi, M. Bordbar, and M. Nasrollahzadeh, J. Colloid Interface Sci. 493 (2017) 85.

[26] A.K. Geim, and K.S. Novoselov, Nanosci. Technol. a Collect. Rev. from Nat. Journals World Scientific (2010) 11.
[27] S. Saxena, and T.A. Tyson, ACS Nano 4 (2010) 3515.
[28] L. Shahriary, and A.A. Athawale, Int. J. Renew. Energy Environ. Eng. 2 (2014) 58.
[29] A.L. Higginbotham, J.R. Lomeda, A.B. Morgan, and J.M. Tour, ACS Appl. Mater. Interfaces 1 (2009) 2256.
[30] A. Lerf, H. He, M. Forster, and J. Klinowski, J. Phys. Chem. B 102 (1998) 4477.
[31] D.C. Marcano, D. V Kosynkin, J.M. Berlin, A. Sinitskii, Z. Sun, A. Slesarev, L.B. Alemany, W. Lu, and J.M. Tour, ACS Nano 4 (2010) 4806.
[32] Z. Alhalili, Arab. J. Chem. 15 (2022) 103739.
[33] D.M. Nzilu, E.S. Madivoli, D.S. Makhanu, S.I. Wanakai, G.K. Kiprono, and P.G. Kareru, Sci. Rep. 13 (2023) 14030.
[34] N. Mahmoud, A. Monireh, S. Mohaddeseh, S.S. Mohammad, and I. Zahra, Plant-Mediated Green Synth. Nanostructures Mech. Charact. Appl. 28 (2019) 199.
[35] M. Halder, M.M. Islam, Z. Ansari, S. Ahammed, K. Sen, and S.M. Islam, ACS Sustain. Chem. Eng. 5 (2017) 648.
[36] M. Nasrollahzadeh, S.M. Sajadi, A. Rostami-Vartooni, and S.M. Hussin, J. Colloid Interface Sci. 466 (2016) 113.
[37] R. Sankar, P. Manikandan, V. Malarvizhi, T. Fathima, K.S. Shivashangari, and V. Ravikumar, Spectrochim. Acta Part A Mol. Biomol. Spectrosc. 121 (2014) 746.
[38] F. Buazar, S. Sweidi, M. Badri, and F. Kroushawi, Green Process. Synth. 8 (2019) 691.
[39] Z.S. Stojanović, E. Mehmeti, K. Kalcher, V. Guzsvány, and D.M. Stanković, Food Anal. Methods 9 (2016) 2701.
[40] F. Zhang, Z. Wang, Y. Zhang, Z. Zheng, C. Wang, Y. Du, and W. Ye, Talanta 93 (2012) 320.
[41] I. Basozabal, A. Guerreiro, A. Gomez-Caballero, M.A. Goicolea, and R.J. Barrio, Biosens. Bioelectron. 58 (2014) 138.
[42] J.C. Myland, and K.B. Oldham, Electrochem. Commun. 6 (2004) 344.